

Surface structure determination of Au(1 ML)/Fe(15 ML)/Au(100) using angle-resolved photoemission extended fine structure

S. A. Kellar

*Department of Chemistry, University of California, Berkeley, California 94720
and Advanced Light Source, Lawrence Berkeley National Laboratory, Berkeley, California 94720*

Y. Chen

Departments of Chemistry and Physics, The Pennsylvania State University, University Park, Pennsylvania 16802

W. R. A. Huff and E. J. Moler

*Department of Chemistry, University of California, Berkeley, California 94720
and Advanced Light Source, Lawrence Berkeley National Laboratory, Berkeley, California 94720*

Z. Hussain

Advanced Light Source, Lawrence Berkeley National Laboratory, Berkeley, California 94720

D. A. Shirley

Departments of Chemistry and Physics, The Pennsylvania State University, University Park, Pennsylvania 16802

(Received 2 May 1997)

We have determined the atomic surface structure of a thin film of Fe (15 ML) grown on the Au(100) surface, Au(1 ML)/Fe(15 ML)/Au(100), with angle-resolved photoemission extended fine structure (ARPEFS) using the Au $4f_{7/2}$ core level. We have confirmed that a bcc crystalline Fe film grows epitaxially on the Au(100) substrate with 1 ML of Au atoms remaining on the surface using angle-resolved photoemission spectroscopy. We analyzed the ARPEFS oscillations using an electron-scattering code based on the Rehr-Albers scattering matrix formalism. Our analysis finds that the surface Au atoms are positioned in the fourfold hollow sites $1.67 \pm 0.02 \text{ \AA}$ above the Fe surface. We also find that the grown Fe layers are very like bulk bcc Fe, with an interlayer spacing of $1.43 \pm 0.03 \text{ \AA}$. [S0163-1829(98)06303-6]

I. INTRODUCTION

A great amount of attention has been given to investigating thin magnetic films and magnetic multilayers, especially systems involving iron and the noble metals.¹⁻⁸ In many of the electronic and magnetic studies the authors assume that the Fe layers will maintain bulk spacing even at interfaces. However, it is well known that for the clean Fe metal, the first and second layer spacing is contracted from the bulk value, and that adsorbates can significantly expand this spacing.⁹⁻²⁰ In addition, there is disagreement in the literature as to the structure of thicker films, especially as to the composition of the topmost layer.^{5,21} Atomic structural details about these interfaces are important because the electronic states that are localized at the interface between the two different materials are critical in determining the magnetic properties of ultrathin films and multilayers.^{22,23} For example, the bonding at the interface induces a magnetic moment in the nonmagnetic material; thus ferromagnetic order is attained in the nonmagnetic noble-metal overlayers on iron. The resulting magnetization is often sizable but decays rapidly away from the interface on the scale of a few atomic layers.²⁴

In this study we use angle-resolved photoemission extended fine structure (ARPEFS) to investigate thin (~ 10 and 15 ML) Fe films grown on a Au(100) single crystal. ARPEFS is a well-established technique for determining the

atomic structure of atomic and molecular adsorbates on metal surfaces.^{18,19,25-28} The technique's advantages are its atomic selectivity due to the unique binding energies of core-level electrons, the large oscillations, which in this study are $\pm 40\%$, and its inherent accuracy. In the past, structural determinations have only been done with ARPEFS signals from initial states with zero angular momentum because of the difficulties in treating non- s initial states in the scattering calculations. This study presents the structure determination of a bimetallic system using the ARPEFS from non- s initial states. We report results from a computer simulation and fitting procedure based on the Rehr and Albers formalism.²⁹ This program, developed by our group, uses second-order matrices (6×6) and up to eighth-order scattering to produce a convergent calculation at these electron energies and interatomic distances.³⁰

II. EXPERIMENT

The experiment was performed at the advanced light source on the bend-magnet beamline 9.3.2, which covers the photon energy range of 30–1500 eV. The ultrahigh vacuum chamber is equipped with a high-precision, five-axis manipulator capable of a temperature range from 80 to 2500 K and other standard surface science techniques for sample preparation and characterization. The photoemission data were collected with a two-axis rotatable, 50-mm mean-radius,

hemispherical, electron-energy analyzer equipped with multichannel detection. The angular resolution of the electron lens system for the analyzer is $\pm 2.0^\circ$. Kevan described the analyzer more completely.³¹

The gold crystal was spark-cut from a high-purity boule and oriented with Laue x-ray back reflection to within $\pm 0.5^\circ$ of the [100] direction. The crystal was mechanically polished with 6- and 1- μm -size diamond paste, and finally with a 0.05- μm CeO₂ slurry. Because gold is very soft, the mechanical polishing steps create a deep, polycrystalline, damaged layer which must be removed in order to obtain high-quality, ordered surfaces. We electropolished the gold crystal to remove this damage layer.³² After repeated cycles of Ar⁺ ion sputtering, $E_k = 500$ eV, $I_e = 10$ μA , and annealing to 550 $^\circ\text{C}$ in vacuum, we could detect no carbon or sulfur, and saw a sharp 5×20 low-energy electron diffraction (LEED) pattern.

The iron source was a 99.999%-purity iron wire heated by electron bombardment. The base pressure in the experimental chamber was 7×10^{-11} torr, while during the evaporation, which lasted 15 min, the pressure rose to 8×10^{-10} torr. To determine the iron coverage, we plotted the gold $4f_{7/2}$ photoemission peak intensity and the iron $3p$ peak intensity against the evaporation time, assigning a value of 1 ML to the first break in the slope of each of these two curves. The bulk iron layer was then grown at room temperature with evaporation times of 10 and 15 times the 1 ML evaporation time, and ARPEFS curves taken of these two samples. After the Fe evaporation, we detected no contaminants on the crystal surface and observed a bright and sharp 1×1 LEED pattern, unrotated relative to the substrate Au(100) face.

The sample temperature, measured with a liquid-nitrogen reference junction and a thermocouple mounted very near the sample, was 80 K for all the work reported here.

III. DATA ANALYSIS

The primary ARPEFS data consist of three sets of Au(4f) photoelectron spectra, two collected in the [100] direction and one collected in the [110] direction. In each data set the photon energies were chosen such that the Au(4f) photoelectron kinetic energies are equally spaced in electron wave number k ; k ranges from 5.3 to 12.0 \AA^{-1} in 0.1 \AA^{-1} steps. Each of the 67 individual photoemission curves for each data set was fitted with a Voigt function and a step function for each peak and a background offset. A Voigt function is the convolution between a Lorentzian describing the peak's natural linewidth and a Gaussian describing the experimental contribution to the peak's width. Figure 1 shows a typical spectrum and fit. We fitted each spectrum in order to extract the most accurate peak intensities from which to construct the $\chi(k)$ diffraction curve. The function $\chi(k)$ is defined by²⁵

$$\chi(k) = \frac{I(k)}{I_0(k)} - 1, \quad (1)$$

where $I(k)$ is each individual peak area plotted as a function of its position in k space. $I_0(k)$ is a smooth, slowly varying function with a much slower oscillation frequency than $I(k)$, which depends on the inelastic scattering processes and the

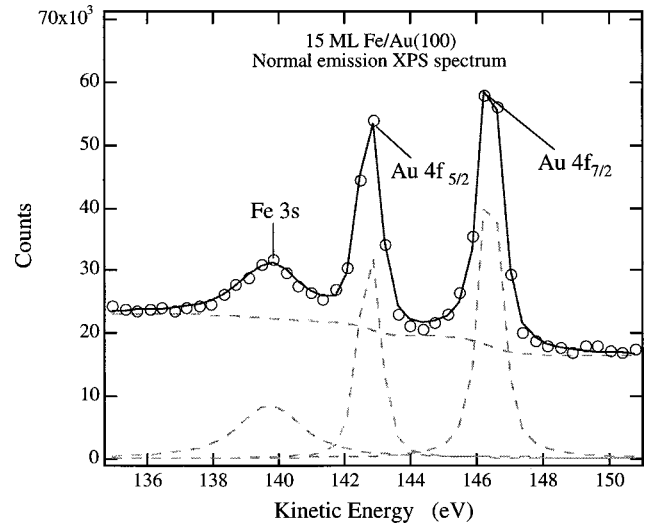


FIG. 1. A typical photoemission spectrum from the 15-ML Fe/Au(100) system. The open circles are the data, the solid line is the fit to the data, and the dashed lines the Voigt function peaks and background.

energy-dependent atomic cross section. We determined $I_0(k)$ by fitting a smooth, cubic spline through the intensity curve. The experimental ARPEFS data thus obtained are plotted in Fig. 2 along with the best-fit results from the multiple-scattering calculations, which are discussed later in this paper.

The generally accepted growth mode of iron on Au(100) is layer by layer with 1 ML of gold, acting as a surfactant, migrating to the surface of the growing iron layer.^{5,7,32} However, Begley *et al.* reported for a Fe-layer thickness of 45 layer equivalents that the topmost layer is not pure Au, but a disordered alloy of Fe and Au.²¹ As other authors have done to test this growth model, at the end of the ARPEFS data collection we lightly sputtered the Fe/Au(100) sample with 200 eV Ar⁺ ions, periodically checking the Fe $3p$ and Au $4f_{7/2}$ peak intensities. After a total sputtering time of 20 min, the Au $4f_{7/2}$ signal was undetectable, the Fe $3p$ was unchanged, and the sample still showed a bright, 1×1 LEED pattern. We also compared the relative Fe $3s$ and Au $4f$ peak intensities from the 15-ML Fe sample.³³ We find the experimental intensity ratio to be $\sim 20\%$ smaller than a theoretical estimate for a monolayer coverage of gold on bulk iron. We take this as further evidence for a single monolayer growth mode, as 20% discrepancy is within the error limits for such a calculation. The absolute intensity of the Au $4f$ signal is also consistent with a Au surface monolayer. We note that the surface free energies of gold (1.410 J/cm²) and iron (2.150 J/cm²) make it thermodynamically favorable for gold to be the surface layer.

The autoregressive linear-prediction-based Fourier transform (ARLP-FT) transforms the diffraction data from momentum space to real space.³³ In ARPEFS, the positions of the strong backscattering peaks in ARLP-FT's from adsorbate/substrate systems can be predicted with fairly good accuracy using the single-scattering cluster model together with the concept of strong backscattering from atoms located within a cone around 180° from the emission direction. The effective solid angle of this backscattering cone is $\sim 30^\circ - 40^\circ$, though signals from scattering atoms very close

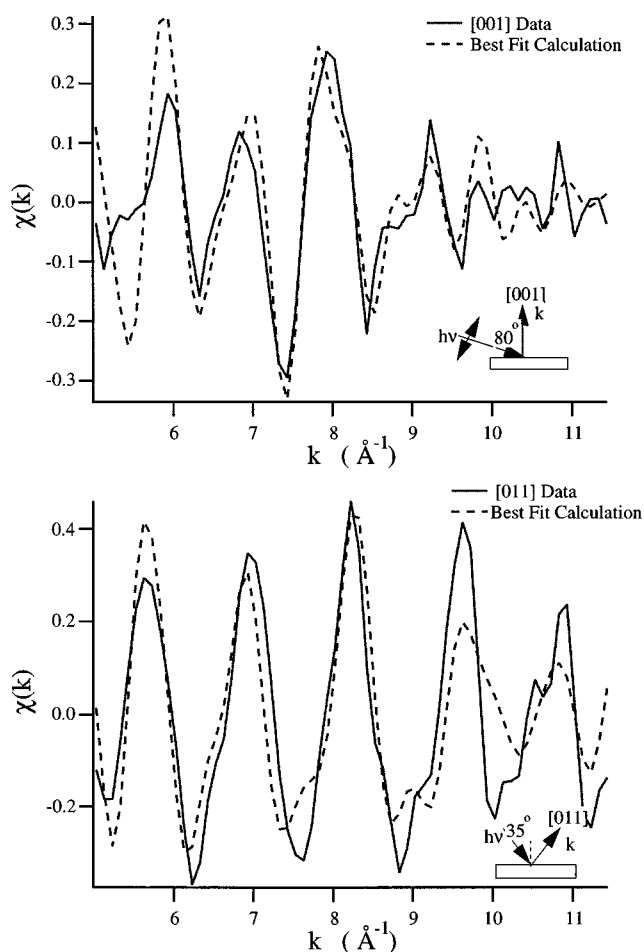


FIG. 2. ARPEFS data from the Au 4*f* core level for 1 ML Au/15 ML Fe/Au(100) in the [001] and [011] directions. Schematics of each experimental geometry are shown. Dashed lines are the best-fit multiple-scattering modeling calculation results. The largest-amplitude oscillations in each curve arise from strong backscattering off the nearest-neighbor Fe atoms in the [001] and [011] directions, respectively. See Fourier transforms in Fig. 3.

to the source atom may be observable even if the scatters lie outside the nominal backscattering cone. Most notably, this applies to the nearest-neighbor Au atoms in the surface layer for this system.

The ARLP-FT peaks correspond to path-length differences between that component of the wave which propagates directly to the detector and those components that are first elastically scattered by the atomic potentials within this backscattering cone. This scattering takes place within the crystal, which requires that the ARPEFS data be shifted to account for the effect of the inner potential. In the modeling calculations, the inner potential is treated as an adjustable parameter, but for the Fourier analysis we estimate its value as the sum of the work function and the valence-band width, which for the present case we take to be 12.6 V. Thus we shifted the ARPEFS data by 12.6 eV to higher kinetic energy before calculating the ARLP-FT.

Analysis of the ARLP-FT provides information about the adsorption site as well as the bonding distance of the gold atoms. The 1×1 LEED pattern suggests a high-symmetry absorption site, and the fact that the lattice constant for bcc iron is a factor of $\sqrt{2}$ smaller than the lattice constant of fcc

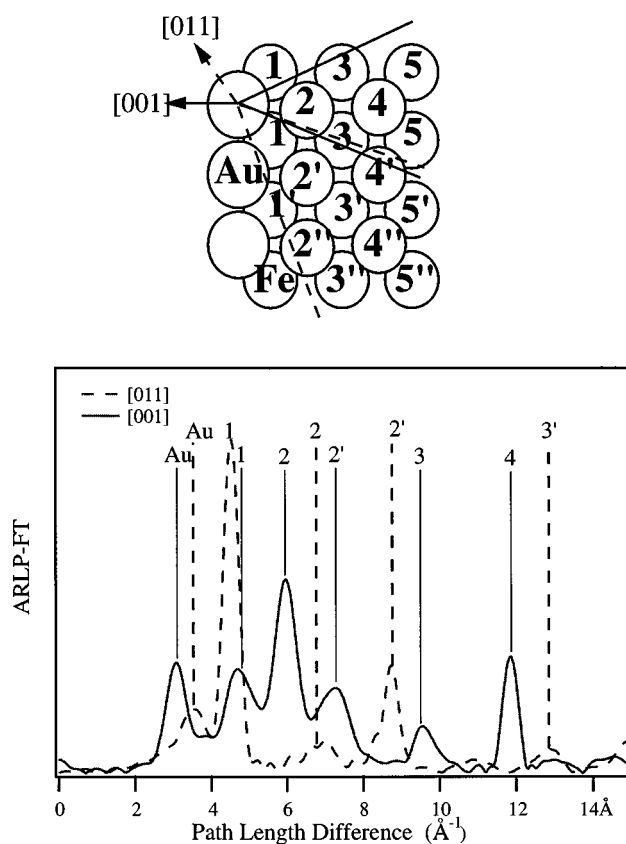


FIG. 3. ARLP-FT's of the ARPEFS [001] data (solid line) and the [011] data (dashed line). A model of the lattice with the backscattering cones for each emission direction indicates the scattering atoms corresponding to the FT peaks. Note the excellent agreement between peak positions and the predicted values on the basis of single scattering and simple geometry.

gold further points to the fourfold hollow as the likely binding site. Using the bulk Fe interlayer spacing, 1.43 Å, and ignoring phase-shift effects, the strongest peak in the [100] ARLP-FT at 6.0 Å can be used as a calibration to calculate the distance between the Au and the first-layer Fe atoms for each high-symmetry absorption site, atop, bridging, or fourfold hollow. Using only plane geometry one can then calculate the path-length differences (PLD) and scattering angles for strong scattering events from each adsorption site geometry and compare them to the observed peaks in the ARLP-FT's. This comparison for both the [100] and [011] emission directions is shown in Fig. 3.

The Fourier analysis agrees best if the Au atoms adsorb in the fourfold hollow ~ 1.57 Å above the first-layer iron. The peak at 6.0 Å corresponds to backscattering from the second-layer iron atoms. For this geometry the predicted and observed PLD are in very good agreement and the relative peak strengths are reasonable for the scattering angles.

Fitting the experimental diffraction curves to a multiple-scattering model yields more precise structural parameters than that given by the Fourier analysis alone. Chen, Wu, and Shirley recently developed a multiple-scattering code, based on the Rehr-Albers formalism, which can model initial states with arbitrary angular momentum and which is fast enough to allow practical fitting to be done.^{29,30} This calculation requires both structural and nonstructural parameters. We used the structural parameters determined by the Fourier analysis

as the initial guesses in the fitting procedure. The nonstructural parameters include the initial-state angular momentum, the atomic scattering phase shifts, the crystal temperature, the inelastic mean free path, the emission and light polarization directions, the electron analyzer acceptance angle, and the inner potential.

To account for the vibrational effects of the bulk atoms, the mean-square relative displacement was calculated and the correlated Debye temperature was set to 265 K. The atomic-scattering phase shifts were calculated using the atomic potentials tabulated by Moruzzi, Janak, and Williams.³⁴ The emission and polarization directions and the analyzer acceptance angle were set to the experimental values described previously.³¹ The inelastic mean free path was included using the exponential damping factor $e^{-t/\lambda}$ where λ was calculated using the Tanuma, Powell, and Penn formula.³⁵

The scattering code allows for several curves of the same initial state to be fitted simultaneously. In this case the two $\chi(k)$ curves from the 15-ML sample with emission along the [100] and [110] directions were fit simultaneously. The [100] emission $\chi(k)$ curve from the 10-ML sample was fitted separately. We determined the best fit by minimizing the A -factor function defined as

$$A = \frac{\sum (\chi_c - \chi_e)^2}{\sum (\chi_c^2 + \chi_e^2)}. \quad (2)$$

We employ the A factor in the fitting routine instead of the conventional R factor because when the fit is far from its minimum the A factor emphasizes the importance of the structurally sensitive $\chi(k)$ curve periodicity, over the absolute peak intensity. Near the minimum the A -factor and R -factor analyses are functionally equivalent. We report the conventional R factor throughout this paper.

We show the experimental $\chi(k)$ curve and the best fit for each emission direction in Fig. 3. For these fits we used an 88-atom cluster and allowed the Au-Fe1, Fe1-Fe2, and Fe2-Fe3 interlayer spacings to vary, as well as the inner potential. During the data analysis it was obvious that, for initial states with orbital angular momentum greater than zero, the diffraction curves are very sensitive to small errors in the measured emission direction. For this reason an iterative process was employed to find the best fit. First, a fitting to the multiple-scattering calculation was performed with the Fourier analysis parameters as the starting structural parameters. The best-fit results of this fitting process were then held fixed as the emission direction in the code was allowed to vary. The resulting best-fit value for the emission angle was then used as the input for the next set of calculations. This iterative process was continued until the emission direction converged. We found that the true emission direction was 4° from that determined experimentally for both the [100] and the [011] directions. We attribute this error to a misalignment of the experimental chamber viewports used in the laser autocollimation orientation procedure.

From the best-fit calculations we determine the Au-Fe1 spacing to be 1.67 Å, and the Fe1-Fe2 and the Fe2-Fe3 spacing to be that of bulk iron, 1.43 Å within the experimental

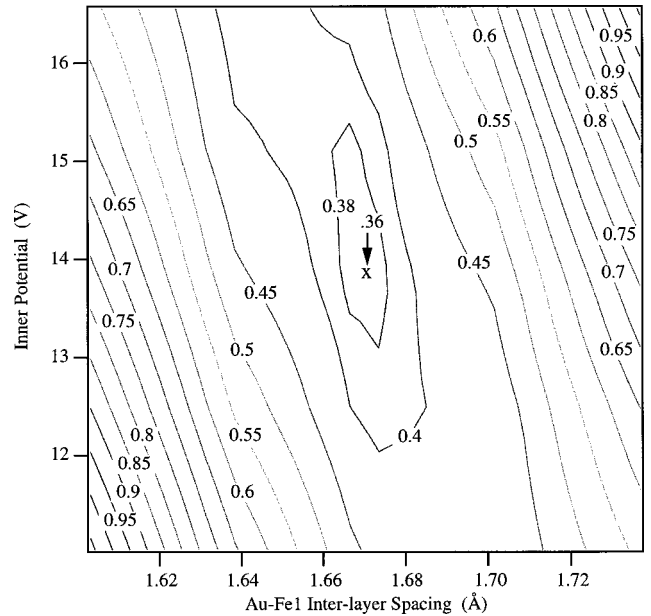


FIG. 4. R factor vs inner potential and Au-Fe1 interlayer spacing. The minimum is at a layer spacing of 1.67 ± 0.02 Å. The Fe1-Fe2 interplanar distance is held constant.

error limits. For the bare Fe metal the Fe1-Fe2 spacing is contracted 1.4% to 1.41 Å.³⁶ A surface Debye temperature of 265 K and an inner potential of 13.8 V were found to give the best fit. The best-fit value for the Debye temperature is noteworthy because it is a measure of the disorder in the system. ARPEFS observes the thermal averaging of the interference effects in which the vibrational motions of the surface atoms attenuate the oscillation amplitude of the $\chi(k)$ function. In the same manner sample imperfections, i.e., intermixing of the gold and iron layers and roughness of the grown iron layers will also attenuate amplitude of $\chi(k)$. Analysis of the ARLP-FT's shows peaks corresponding to scattering events from as far away as the fourth iron layer. Wang *et al.* showed previously that information from such large PLD is lost as the sample temperature approaches the Debye temperature, that is, as the sample becomes more disordered.^{37,38} The fact that we see such long PLD's is another indication of the quality of the iron films and the sharpness of the iron-gold interface. The very good agreement between the predicted and the observed peaks in the ARLP-FT and the presence of sharp ARLP-FT peaks due to scattering from the fourth Fe layer, provides strong and direct evidence that the Fe film is essentially identical to that of bulk bcc Fe.

IV. ERROR ANALYSIS

To establish the sensitivity of the fitting procedure to the layer spacings and establish error bars we calculated the R factor for the various interlayer spacings and inner potential. It has been shown that the inner potential may affect the derived layer spacings and must be included in the R -factor analysis.²⁸ Figure 4 shows the R -factor contours versus the Au-Fe1 layer spacing and inner potential. Figure 5 shows the similar plot for the first-layer and second-layer Fe spacing and the inner potential. These plots show a very steep valley

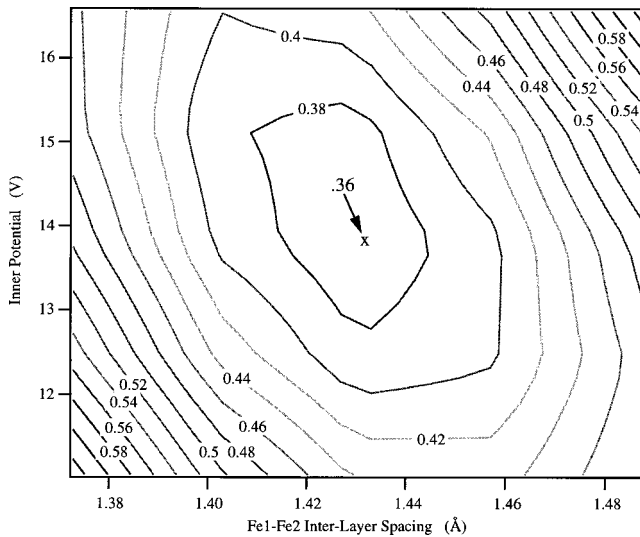


FIG. 5. R factor vs inner potential and Fe1-Fe2 interlayer spacing. The minimum is at an interlayer spacing of 1.43 ± 0.03 Å.

in the interlayer spacing direction with a very broad valley floor in the inner potential direction, indicating the relative insensitivity of the fits to the inner potential value. With the inner potential held fixed at the best-fit value of 13.8 V the R -factor analysis for the gold first-layer spacing, first-layer iron second-layer iron, and second-layer iron third-layer iron are shown in Fig. 6. Huang discussed the determination of error bars in ARPEFS from the R -factor analysis.²⁷ Following his treatment we quote errors of plus or minus one standard deviation. We conclude from the multiple-scattering spherical wave calculation and the R -factor analysis that the Au-Fe1 spacing is 1.67 ± 0.02 Å, the Fe1-Fe2 spacing is 1.43 ± 0.03 Å, and the Fe2-Fe3 spacing is 1.46 ± 0.05 Å.

V. CONCLUSION

We have measured the Au $4f$ ARPEFS signal from 1 ML Au/15 ML Fe/Au(100) and find that the iron grows layer by layer with 1 ML of Au sitting in the fourfold hollow site of the bcc iron. We contrast this finding with that of Begley *et al.* who reported that surface layer of the 45 layer-equivalent Fe film was not pure Au, but a disordered alloy of Au and Fe. It may well be that thicker films are more disordered. We find that the layer spacing between the top gold layer and the first iron layer is 1.67 ± 0.02 Å, the spacing between the first- and second-layer iron atoms is 1.43 ± 0.03 Å, and the interlayer spacing for second- and third-layer iron atoms is 1.46 ± 0.05 Å. The Fourier analysis and the multiple-scattering calculations indicate that the growing

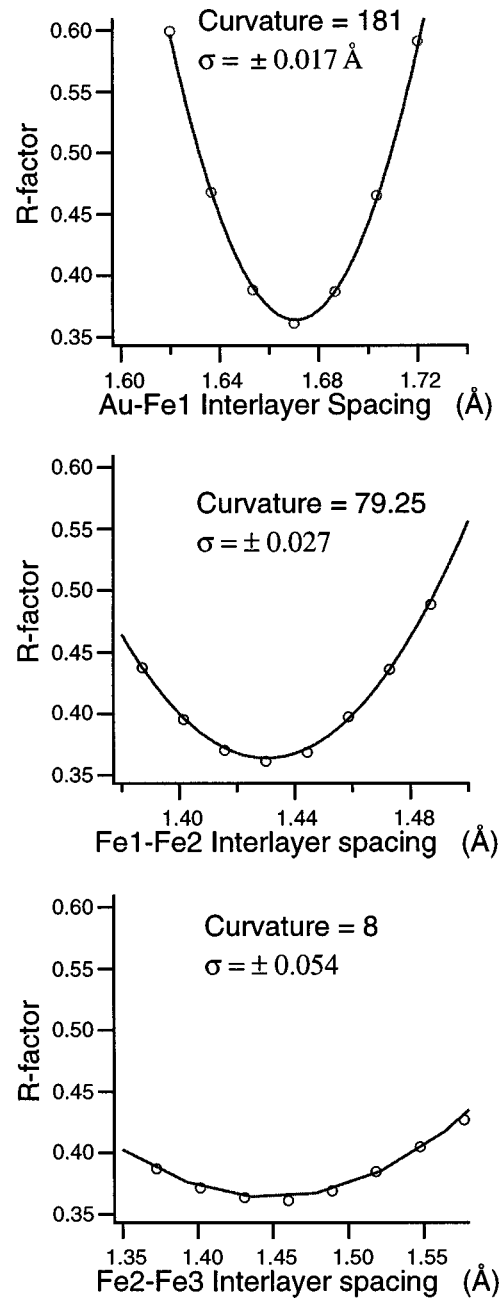


FIG. 6. R factor vs the interlayer spacing (open circles) and a parabolic fit (solid line) for (A) Au-Fe1, (B) Fe1-Fe2, and (C) Fe2-Fe3. The inner potential is fixed at 13.6 V for all calculations.

iron layers are very like equilibrium bulk Fe with a bcc lattice. We have also demonstrated a new multiple-scattering code and fitting procedure based on the Rehr-Albers formalism that can calculate up to eighth-order scattering, using 6×6 scattering matrices rapidly enough to allow practical fitting to be done.

¹F. Ciaccacci and S. D. Rossi, Phys. Rev. B **51**, 11 538 (1995).

²E. Vescovo, O. Rader, J. Redinger, S. Blugel, and C. Carbone, Phys. Rev. B **51**, 12 418 (1995).

³F. J. Himpsel, Phys. Rev. B **44**, 5966 (1991).

⁴J. M. Maclaren, M. E. McHenry, S. Crampin, and M. E. Eberhart, J. Appl. Phys. **67**, 5406 (1990).

⁵S. D. Bader and E. R. Moog, J. Appl. Phys. **61**, 3729 (1987).

⁶W. Gerts, Y. Suzuki, T. Katayama, K. Tanaka, K. Ando, and S.

- Yoshida, Phys. Rev. B **50**, 12 581 (1994).
- ⁷Y.-L. He, Y.-F. Liew, and G.-C. Wang, J. Appl. Phys. **75**, 5580 (1994).
- ⁸W. Heinen, C. Carbone, T. Kachel, and W. Gudat, J. Electron Spectrosc. Relat. Phenom. **51**, 701 (1990).
- ⁹W. Arabczyk, H.-J. Müssig, and F. Storbeck, Surf. Sci. **251/252**, 804 (1991).
- ¹⁰W. Arabczyk, T. Baumann, F. Storbeck, H. J. Müssig, and A. Meisel, Surf. Sci. **189/190**, 190 (1987).
- ¹¹S. R. Chubb and W. E. Pickett, Solid State Commun. **62**, 19 (1987).
- ¹²S. R. Chubb and W. E. Pickett, Phys. Rev. B **38**, 10 227 (1988).
- ¹³R. Imbihl, R. J. Behm, G. Ertl, and W. Moritz, Surf. Sci. **123**, 129 (1982).
- ¹⁴K. O. Legg, F. Jona, D. W. Jepsen, and P. M. Marcus, Phys. Rev. B **16**, 5271 (1977).
- ¹⁵K. O. Legg, F. Jona, D. W. Jepsen, and P. M. Marcus, Surf. Sci. **66**, 25 (1977).
- ¹⁶R. S. Saiki, G. S. Herman, M. Yamada, J. Osterwalder, and C. S. Fadley, Phys. Rev. Lett. **63**, 283 (1989).
- ¹⁷S. Tang, A. J. Freeman, and G. B. Olson, Phys. Rev. B **47**, 2441 (1993).
- ¹⁸W. R. A. Huff *et al.*, Phys. Rev. B **55**, 10 830 (1997).
- ¹⁹X. S. Zhang, L. J. Terminello, S. Kim, Z. Q. Huang, A. E. S. v. Wittenau, and D. A. Shirley, J. Chem. Phys. **89**, 6538 (1988).
- ²⁰J. M. V. Zoest, J. M. Fluit, T. J. Vink, and B. A. V. Hassel, Surf. Sci. **182**, 179 (1987).
- ²¹A. M. Begley, S. K. Kim, J. Quinn, F. Jona, H. Over, and P. M. Marcus, Phys. Rev. B **48**, 1779 (1993).
- ²²A. J. Freeman and R. Wu, J. Magn. Magn. Mater. **100**, 497 (1991).
- ²³L. H. Bennet and R. E. Watson, *Magnetic Multilayers* (World Scientific, Singapore, 1993).
- ²⁴K. Totland, P. Fuchs, J. C. Groebli, and M. Landolt, Phys. Rev. Lett. **70**, 2487 (1993).
- ²⁵J. J. Barton, S. W. Robey, and D. A. Shirley, Phys. Rev. B **34**, 778 (1986).
- ²⁶J. J. Barton, C. C. Bahr, S. W. Robey, Z. Hussain, E. Umbach, and D. A. Shirley, Phys. Rev. B **34**, 3807 (1986).
- ²⁷Z. Huang, Ph.D. thesis, University of California, Berkeley, 1992.
- ²⁸W. R. A. Huff, Y. Zheng, and Z. Hussain (unpublished).
- ²⁹J. J. Rehr and R. C. Albers, Phys. Rev. B **41**, 8139 (1990).
- ³⁰Y. F. Chen, W. Wu, and D. A. Shirley (unpublished).
- ³¹S. D. Kevan, Ph.D. thesis, The University of California, Berkeley, 1980.
- ³²R. Germar, W. Durr, J. W. Krewer, D. Pesdia, and W. Gudat, Appl. Phys. A: Solids Surf. **47**, 393 (1988).
- ³³J. J. Barton, Ph.D. thesis, The University of California, Berkeley, 1985.
- ³⁴V. L. Moruzzi, J. F. Janak, and A. R. Williams, *Calculated Electronic Properties of Metals* (Pergamon, New York, 1978).
- ³⁵S. Tanuma, C. J. Powell, and D. R. Penn, Surf. Interface Anal. **11**, 577 (1988).
- ³⁶K. O. Legg, F. Jona, D. W. Jepsen, and P. M. Marcus, Phys. Rev. B **16**, 5271 (1977).
- ³⁷L.-Q. Wang *et al.*, Phys. Rev. B **44**, 13 711 (1991).
- ³⁸L.-Q. Wang *et al.*, Phys. Rev. B **44**, 1292 (1991).